ACS OMEGA

http://pubs.acs.org/journal/acsodf

Article

Phase Volume Fraction-Dependent Strengthening in a Nano-Laminated Dual-Phase High-Entropy Alloy

Cheng Huang, Yin Yao,* and Shaohua Chen*

Cite This: *ACS Omega* 2022, 7, 29675−29683

Read Online

ACCESS | Metrics & More | Article Recommendations | Supporting Information

ABSTRACT: A recently synthesized FCC/HCP nano-laminated dual-phase (NLDP) CoCrFeMnNi high entropy alloy (HEA) exhibits excellent strength−ductility synergy. However, the underlying strengthening mechanisms of such a novel material is far from being understood. In this work, large-scale atomistic simulations of in-plane tension of the NLDP HEA are carried out in order to explore the HCP phase volume fraction-dependent strengthening. It is found that the dual-phase (DP) structure can significantly enhance the strength of the material, and the strength shows apparent phase volume fraction dependence. The yield stress increases monotonously with the increase of phase volume fraction, resulting from the increased inhibition effect of interphase boundary (IPB) on the nucleation of partial dislocations in the FCC lamella. There exists a critical phase volume fraction, where the flow stress is the largest. The mechanisms for the volume fraction-dependent flow stress include volume fraction-dependent phase strengthening effect, volume fraction-dependent IPB strengthening effect, and volume fraction-dependent IPB softening effect, that is, IPB migration and dislocation nucleation from the dislocation−IPB reaction sites. This work can provide a fundamental understanding for the physical mechanisms of strengthening effects in face-centered cubic HEAs with a nanoscale NLDP structure.

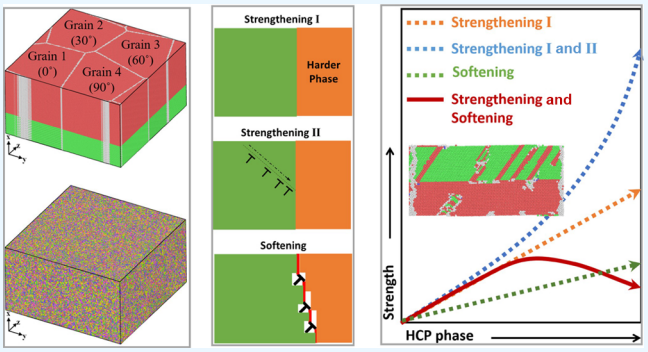

1. INTRODUCTION

The rapid development of modern industry has put forward higher requirements for the comprehensive performance of engineering metals. Many effective strategies have been proposed for improving the performance of engineering metals, such as microstructure optimization design[1−4] and alloying methods,[5−7] among which the alloying strategy commonly based on a single primary element has tended to be the bottleneck of performance. At the beginning of this century, a kind of novel alloying strategy based on several primary elements was proposed, which broke the limitations of traditional methods.[8,9] The novel alloys are generally named as high/medium entropy alloys (HEAs/MEAs) because of their high configurational entropy, which often form compositionally complex solid solutions instead of intermetallic compounds.[10−12] In the past years, HEAs have attracted more attention and interest due to their excellent properties and performances, especially mechanical properties,[13−15] such as superior strength and hardness,[16−18] outstanding fracture toughness and ductility,[19,20] and remarkable resistance to friction and wear.[21]

The mechanical properties of HEAs can be obviously affected by their components, solid solution phases, and multiscale microstructures.[22] For example, adding oxygen atoms into a HEA can form ordered oxygen complexes, which can significantly strengthen and toughen the material.[23] Replacing manganese atoms in CoCrFeMnNi HEA with palladium atoms can considerably increase the difference in atomic size and decrease the homogeneity, which is an effective route to increase the yield strength of HEAs without loss of strain hardening and tensile ductility.[24] A short range order structure is observed in CoCrNi MEA and has been found to give rise to both higher stacking fault energy and hardness.[18] Introduction of nanoprecipitates into an MEA has been proven to improve both the strength and ductility of the material.[25] The nanoprecipitates can not only hinder the movement of dislocations, but also modulate the process of FCC to BCC phase transformation, which are responsible for the strengthening and toughening.

In addition to the abovementioned strengthening and toughening strategies, the recently reported dual-phase (DP) structure can make HEAs reach good strength−ductility synergy.[26−28] For instance, the synthesized $Fe_{50}Mn_{30}Co_{10}Cr_{10}$ HEA exhibits a DP structure with ∼28% HCP phase and

Received: April 1, 2022
Accepted: August 5, 2022
Published: August 18, 2022

https://doi.org/10.1021/acsomega.2c02027
ACS Omega 2022, 7, 29675−29683

~72% FCC matrix phase,[29] which leads to an apparent increase of both tensile strength and ductility. Similarly, the $Co_{20}Cr_{20}Fe_{40-x}Mn_{20}Ni_x$ HEAs with x = 0−20% with a DP structure are designed.[30] The volume fraction of HCP phase can be tailored by varying Ni content. For instance, when x = 6, the volume fraction of HCP phase is 6%. The obtained DP HEA exhibits higher ultimate tensile strength as well as strain-hardening ability compared to the equi-atomic CoCrFeMnNi HEA. The as-cast $Fe_{67}Co_{8.25}Cr_{8.25}Ni_{8.25}Mn_{8.25}$ HEA is composed of FCC and BCC phases, and the FCC phase can transform into a martensitic BCC phase under external loading. Except for the high ultimate tensile strength, the DP HEA exhibits high strain-hardening ability with a rate of 4.1.[31] In addition, the DP structure can also be introduced into equi-atomic CoCrFeMnNi HEA by high-pressure processing 32. Depressurization from 54.1 GPa yields a volume fraction of HCP phase of 56.2% at ambient conditions, while depressurization from 28.6 GPa yields a volume fraction of HCP phase of 34.1% at ambient conditions.

The aforementioned DP structure is a kind of microstructure where different phases are distributed in different grains. Recently, another kind of DP structure that contains nano-laminated FCC and HCP phases is reported. Load-driven formation of nano-laminated DP (NLDP) HEA is achieved, and the ultimate tensile strength and uniform elongation are largely improved compared with single-phase HEA.[33] A Cantor-like $Cr_{20}Mn_6Fe_{34}Co_{34}Ni_6$ alloy has a NLDP structure with a minimum lamella thickness of only several nano-meters, and the strain hardening is greatly increased with assistance of a transformation-induced plasticity effect.[34] The route of mechanically induced FCC to HCP transformation in CrCoNi MEA can also reach the NLDP structure, and the atomic stacking between adjacent FCC and HCP lamellas is $(111)_{FCC}//(0001)_{HCP}$.[27,35] When under plastic deformation, the NLDP HEA undergoes transformation of HCP, nano-twinned NLDP, and nano-twinned FCC, which makes great contributions to strength and toughness. A similar NLDP structure is also found in CoCrFeMnNi HEA. Zhao et al.[36] prepared the DP HEA through swaging, followed by quasi-static compression or dynamic deformation in shear. The propagation of nucleated stacking faults and deformation twins generates high-deformation regions, which can reorganize into hexagonal packets, that is, NLDP structure.

To date, most of the studies have been performed with experiments and first-principles calculations, and there has been little information about the mechanical details of deformation and strengthening from these research studies.[37] It is well known that molecular dynamics (MD) simulations can bridge the gap between macro-scale mechanical properties and underlying physical mechanisms.[38−41] In this work, large-scale MD simulations are adopted to gain insights into the phase volume fraction-dependent strengthening mechanisms of the NLDP HEAs.

2. ATOMISTIC SIMULATION APPROACH

An experimental sample[34] of the polycrystalline (PC) NLDP HEA with coherent interphase boundaries (IPBs) is shown in Figure 1a. Correspondingly, a representative PCNLDP HEA atomistic model with a random solid solution (RSS) structure[42] is constructed in Figure 1b, where the atoms in the upper row of pictures with five different colors represent five elements, and the atoms in the lower row of pictures are colored with green for the FCC structure, red for the HCP structure, and white for the disordered structure. It should be noted that considering the limitation of computing ability of MD simulation, we therefore simplify the numerical model to nanoscale PC, which would not affect our main purpose of studying the effect of volume fraction of nanoscale phases on the deformation of the HEA. The calculated lattice constant of FCC phase is a = 3.595 Å, and those of HCP phase are a = 2.544 Å and c = 4.143 Å, respectively, consistent with the experimental values.[32] The relationships of lattice orientation between the two phases are set according to the experimental observations.[33,34] Each sample includes four grains with a mean grain size of 20 nm. The lattice orientation of grain 1 is $x//[\bar{1}\bar{1}1]_{FCC}//[0001]_{HCP}$, $y//[110]_{FCC}//[1\bar{2}10]_{HCP}$, and $z//[\bar{1}\bar{1}2]_{FCC}//[10\bar{1}0]_{HCP}$, that is, following the Shoji-Nishiyama orientation relationship.[43] Grains 2, 3, and 4 are obtained by rotating grain 1 about the x axis from the z axis by 30°, 60°, and 90° clockwise, which renders all grain boundaries to be high angles. This treatment is commonly used in atomistic simulations.[1,2,44] The dimension of each sample is 22.4, 40, and 40 nm in x, y, and z directions. To study the effect of HCP phase volume fraction (f), NLDP samples with f = 0, 16.67, 33.33, 50, 66.67, 83.33, and 100% are constructed by changing the layer thicknesses of FCC and HCP phases.

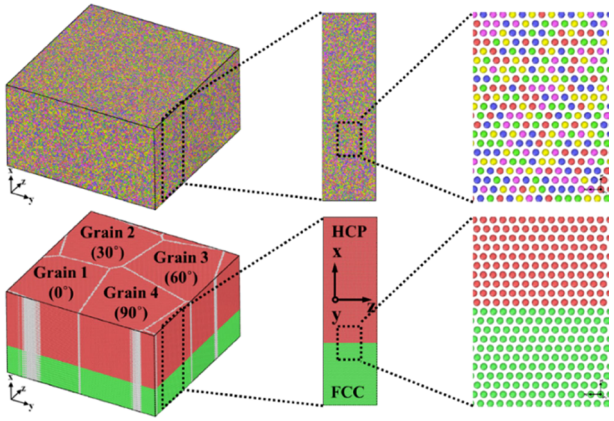

Figure 1. Simplified numerical model for atomistic simulations of in-plane tension of PCNLDP HEA, where the atoms in the upper row of pictures with five different colors represent five different elements (Co, Cr, Fe, Mn, and Ni), and the atoms in the upper row of pictures are colored with green for the FCC structure, red for the HCP structure, and white for the disordered structure.

MD simulations are performed with LAMMPS,[45] and the well-validated MEAM potential[46] is used. This potential has been widely adopted in describing the physical and mechanical properties of the FCC-phased CoCrFeMnNi alloy system[47,48] and is also used in FCC/HCP DP CoCrFeMnNi alloy systems.[26,49,50] In addition, to further verify the reliability of the potential function, we calculate the lattice constant, cohesive energy, elastic properties, and stacking fault energy of the HCP-phased CoCrFeMnNi HEA by means of MD simulations and compare the results with those of first-principles calculations (see Supporting Information for more details). The atomistic models are first optimized by the conjugate gradient algorithm and then annealed at 600 K for reaching the thermodynamic steady state. The annealed samples are finally tensioned along the y direction, that is, in-plane tension, with a strain rate of 0.5/ns and a temperature of 300 K under an NPT ensemble. Nanoscale deformation analysis is carried out with OVITO,[51] in which dislocation

https://doi.org/10.1021/acsomega.2c02027
ACS Omega 2022, 7, 29675−29683

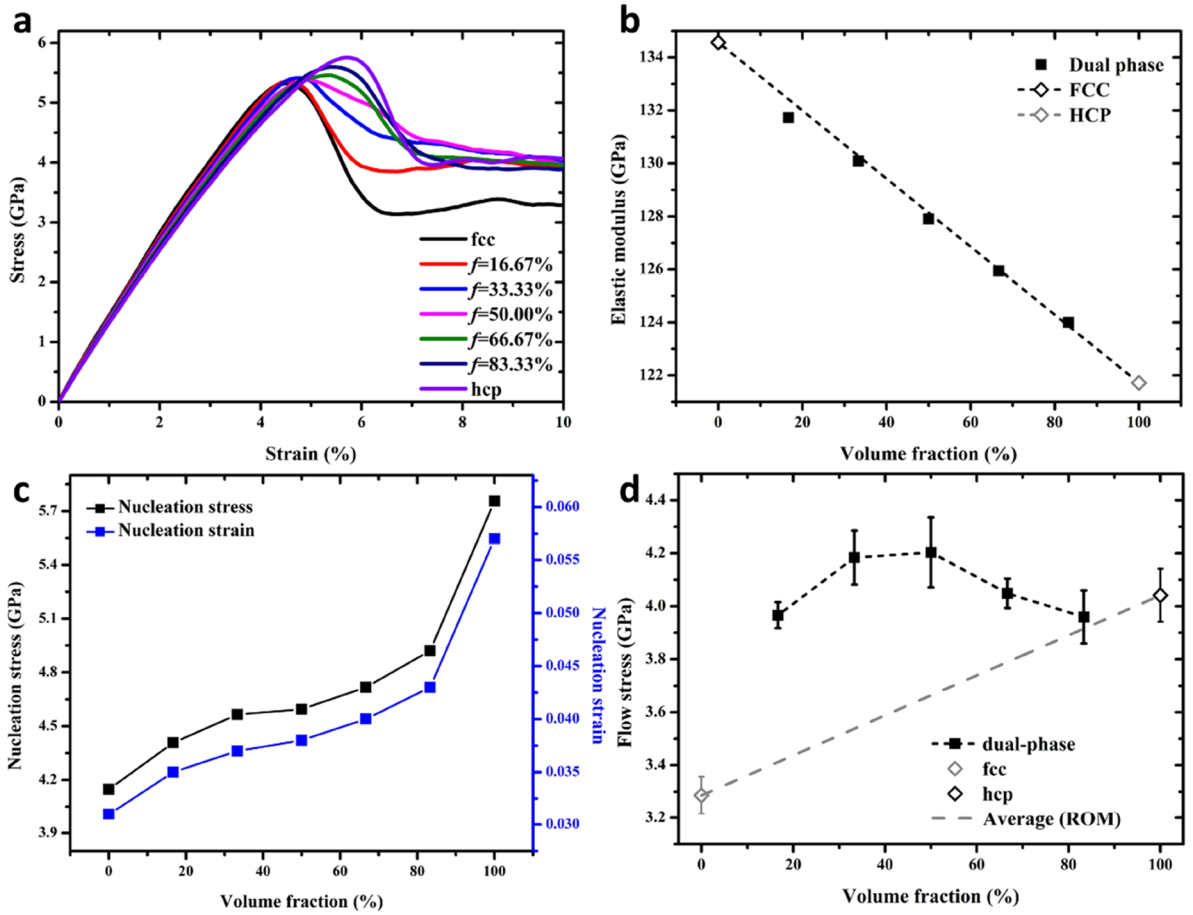

Figure 2. Tensile mechanical responses of the PCNLDP HEAs with different phase volume fractions. (a) Stress−strain ($\sigma-\varepsilon$) curves, (b) Young's modulus, (c) yield stress and yield strain, and (d) flow stress.

extraction algorithm (DXA)[52] and polyhedral template matching[53] methods are included.

3. RESULTS AND DISCUSSION

3.1. Tensile Mechanical Responses. The tensile mechanical responses for the PCNLDP HEAs with various HCP phase volume fractions are shown in Figure 2, and those of the single stable FCC and meta-stable HCP phases are also given for comparison. Figure 2a gives the stress−strain curves. When the loading is applied, the tensile stress is different for different samples at certain strain during the whole elastic and plastic regions, exhibiting remarkable phase volume fraction dependence of mechanical properties. On the other hand, each curve undergoes elastic yielding and shows plastic flow behaviors. The tensile stresses for PCNLDP HEAs during the yielding and plastic flow stages are much higher than those of pure FCC single-phase PC HEA, indicating the DP strengthening effect.

The Young's modulus, taking the slope of the stress−strain curve within a strain range of 0−1%, of the PCNLDP HEAs versus phase volume fraction is shown in Figure 2b. The Young's moduli of FCC and HCP phases are denoted as E_{FCC} and E_{HCP}, and the volume fraction of HCP phase is marked as f. Then, Young's modulus of the PCNLDP HEAs, E, can be described with the rule of mixture as

$$E = E_{HCP}f + E_{FCC}(1-f) = E_{FCC} + (E_{HCP} - E_{FCC})f \quad (1)$$

Eq 1 implies a linear relationship between Young's modulus of the PCNLDP HEAs and the phase volume fraction and can fit well with the obtained MD results. Thus, Young's modulus of the PCNLDP HEAs decreases linearly with the increase of volume fraction of HCP phase.

The yielding behavior of metallic materials is the result of nucleation of dislocations in the interior of grains. Thus, the yield stress can also be regarded as the stress needed for dislocation nucleation. Figure 2c plots the yield stress as a function of HCP phase volume fraction. It can be seen that both the yield stress and yield strain increase with the increase of phase volume fraction, indicating a phase volume fraction-dependent yield stress strengthening.

In order to intuitively reveal the sensitivity of flow stress of the PCNLDP HEA samples to phase volume fraction, we calculate the mean of flow stress for each sample by taking the average of stress between ε = 6 and 10%, noting that in this stage, plastic flow takes place in all samples. Figure 2d shows the variation of flow stress of the PCNLDP HEAs with f, and those of the single-phase FCC and HCP HEAs are also presented for comparison. The flow stresses of the PCNLDP HEAs are obviously higher than those of the stable FCC phase, indicating a remarkable phase strengthening effect. The variation of flow stress of the PCNLDP HEA with the volume fraction does not show a monotonous relationship, which is totally different from that of the nucleation stress. The latter is only related to the nucleation of partial dislocations in the FCC lamella, while the former could be related to the complicated

https://doi.org/10.1021/acsomega.2c02027
ACS Omega 2022, 7, 29675−29683

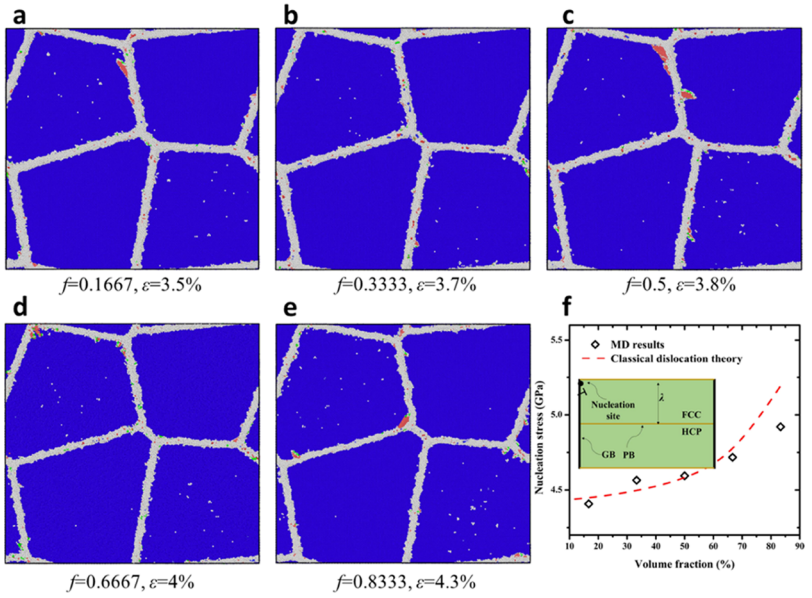

Figure 3. Nucleation of dislocations in the PCNLDP HEAs. (a−e) Perspective view of nucleation of partial dislocations in the FCC lamella. In the figures, the blue atoms in the lower layer represent HCP nano-lamella, the red atoms in the upper layers denote nucleated stacking faults, the atoms colored with white represent grain boundaries and dislocation cores, and the atoms with a perfect FCC lattice in the upper layer are deleted for clarity. The Shockley partial dislocations are colored with green lines. (f) Critical stress for nucleation of Shockley partial dislocation as a function of phase volume fraction.

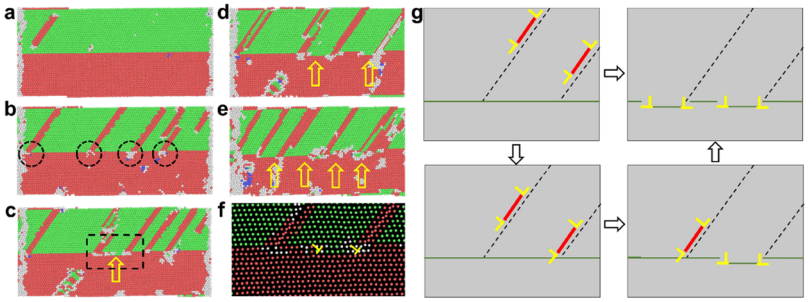

Figure 4. Interaction between glide dislocations and coherent IPB. (a−e) Atomic snapshots of the interaction process. (f) Enlarged view of the square region in (c). (g) Schematic diagram for the IPB migration induced by the interaction.

dislocation activities in both FCC and HCP lamellas, as well as the IPBs.

3.2. Dislocation Nucleation in FCC Lamella. Figure 4 shows the nucleation of Shockley partial dislocations in the PCNLDP HEAs with different volume fractions of HCP phase. For all the samples, Shockley partial dislocations, associated with stacking faults, primarily nucleate from the random high angle grain boundaries of FCC phase, while the HCP phase has not yet yielded. With the increase of the volume fraction, that is, the decrease of the thickness of FCC lamella, the effective distance between the nucleation sites and the IPB decreases, leading to the delay of emergence of partial dislocations. It is generally accepted that the possibility of dislocation nucleation in nano-structured materials would be affected by the distance between the nucleation sites and the obstacles such as twin boundaries, PBs, grain boundaries, dislocation walls, and so on.[54−56] The required critical shearing stress τ_s to emit a partial dislocation is

$$\tau_s = \frac{\gamma}{b} + \frac{Gb}{3\lambda} \quad (2)$$

where G, b, γ, and λ are the shear modulus of a material, the magnitude of the Burger vector of the Shockley partial dislocation, the stacking fault energy, and the distance between the nucleation site and the obstacle, respectively. Here, λ is regarded as the thickness of the FCC lamella since dislocations first nucleate within the FCC lamella, which is also written as $\lambda = f L_x$. Then, according to the Schmid's law $\tau = M\sigma$, where M is the Schmid's factor, the critical tensile stress σ_s can be obtained. For the HEA, G = 83.76 GPa, b = 0.14676 nm, γ = 0.24 J/m^2, and M = 0.392. Thus, a theoretical prediction of volume fraction-dependent stress for dislocation nucleation can be obtained, as shown in Figure 3f. The relationships between the nucleation stress and volume fraction of HCP phase obtained through MD simulations and classical dislocation theory show the same trend, indicating that IPB and HCP volume fractions are responsible for the volume fraction-dependent stress for dislocation nucleation.

3.3. Dislocation−IPB Interaction. To clarify the underlying mechanisms for the DP strengthening effect on flow stress (Figure 2d), it is essential to clarify the plastic deformation in the NCNLDP HEAs. The plastic deformation in the NCNLDP structure should be mediated by the coherent

https://doi.org/10.1021/acsomega.2c02027
ACS Omega 2022, 7, 29675−29683

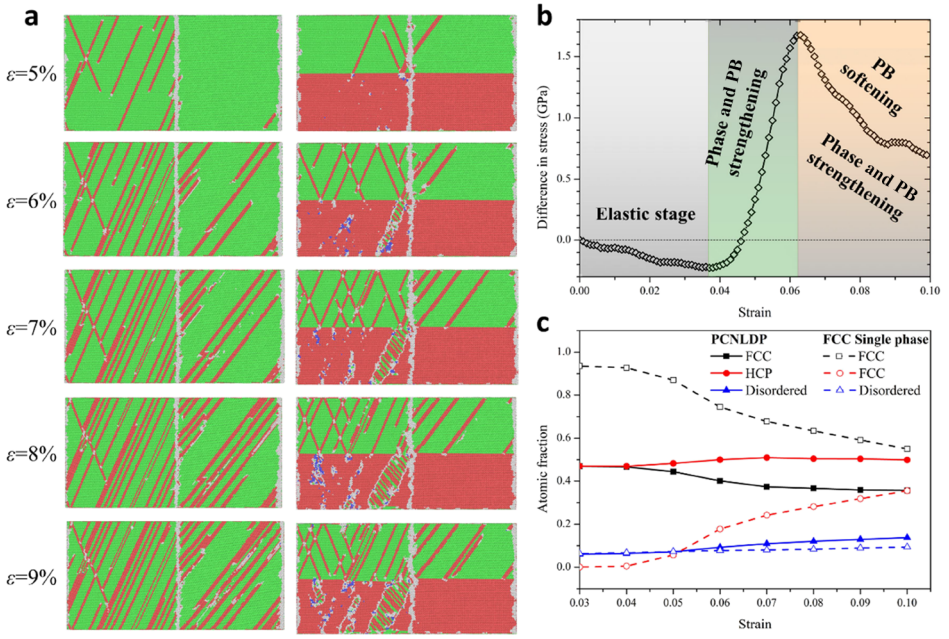

Figure 5. Comparative plastic deformations in PCNLDP and FCC single-phased HEAs. (a) Crystal defects evolutions in the two samples at different strains. (b) Variation of difference in stress between the two samples during deformation. (c) Variations of atomic fractions of FCC-structured, HCP-structured, and disordered atoms with applied strain in the two samples.

IPB. Thus, we first shed light on the interaction mechanism between the glide dislocations and the coherent IPB. Figure 4 presents the local structure evolution in a NCNLDP HEA. Dislocations and stacking faults first nucleate in the FCC lamella from the random high angle grain boundary and then glide toward the IPB (Figure 4a). Due to the difference in physical properties and crystallographic relationships between the two phases, the dislocations in the FCC lamella are blocked by the coherent IPB (Figure 2b). Unlike a nano-twinned structure, the dislocations in the NLDP structure cannot directly cut across the IPB and transmit into the lower HCP lamella. With further straining, the blocked dislocations are absorbed into the coherent IPB (Figure 4c,f), where dislocations can easily glide to leave room for subsequent absorption. Then, the glide of partial dislocations drives the migration of initially coherent IPB, leaving steps in the IPB (Figure 4d,e). The migration of coherent interfaces or boundaries is generally thought of as a kind of deformation mode that softens a material.[57] Figure 4g gives the schematic diagram for the dislocation−IPB interaction and the associated IPB migration.

3.4. DP Strengthening Mechanism. Introduction of HCP phase and coherent IPB leads to significant enhancement of strength of the CoCrFeMnNi HEA (Figure 2). To reveal the underlying mechanism for the DP strengthening effect, we shown in Figure 5 the comparative study on the plastic behaviors of a PCNLDP HEA sample and the FCC single-phased sample. The left column of Figure 5a is the deformation of the FCC single-phased sample, where it can be seen that Shockley partial dislocations and stacking faults can move in the grains, which is only confined by the random high angle grain boundaries. The deformation in the PCNLDP sample is quite different (the right column of Figure 5a). The dislocations and stacking faults nucleate first in the FCC phase from the random high angle grain boundaries, and the amount of crystal defects in the HCP lamella is much less than that in the FCC lamella. It means that HCP lamellas are harder domains in the PCNLDP HEAs, which can lead to a phase strengthening effect. Moreover, the movements of dislocations in the FCC lamella are heavily confined by the IPBs due to the fact of nanoscale PB spacing (ε = 5% in Figure 5a), which results in an apparent IPB strengthening. As emphasized in Figure 4, the blocked dislocations react with the coherent IPB, resulting in the migration of coherent IPB, which can in turn act as sources for dislocation nucleation (ε = 6% in Figure 5a). The deformation twins and dislocations nucleate and propagate in the HCP lamella from the sources (ε = 6−10%). The deformation twins are mainly 10−11> nano-twins, and the dislocations include both basal 0001> and nonbasal 10−11> slips along 1/3<1−210>, <1−100>, and 1/3<1−100> slip directions, which are consistent with the previous experiment.[58] The IPB migration and dislocation nucleation from the reaction sites are softening factors for the strength of the material.

The abovementioned analysis on the deformation of the two samples indicates that the strength of the NLDP HEA is modulated by both strengthening effects, that is, phase strengthening and IPB strengthening and softening effects, that is, IPB migration and dislocation nucleation from the reaction sites. We show in Figure 5b the variation of difference in stress between the two samples during deformation where obvious strengthening and softening effects are confined. In addition, the stacking faults and phase transformations in FCC phase are recognized as double-layered and multilayered HCP-structured atoms, the stacking faults and phase transformations in HCP phase are recognized as double-layered and multi-layered FCC-structured atoms, and the dislocation cores and amorphizations in both phases are recognized as disordered atoms. Thus, we compute the variations of atomic fractions of FCC-structured, HCP-structured, and disordered atoms with applied strain in the two samples for further comparison of the deformation, as shown in Figure 5c. The dotted lines donate variations of atomic fractions in the FCC-phased sample. The rapid decrease of FCC-structured atoms corresponds to the

https://doi.org/10.1021/acsomega.2c02027
ACS Omega 2022, 7, 29675−29683

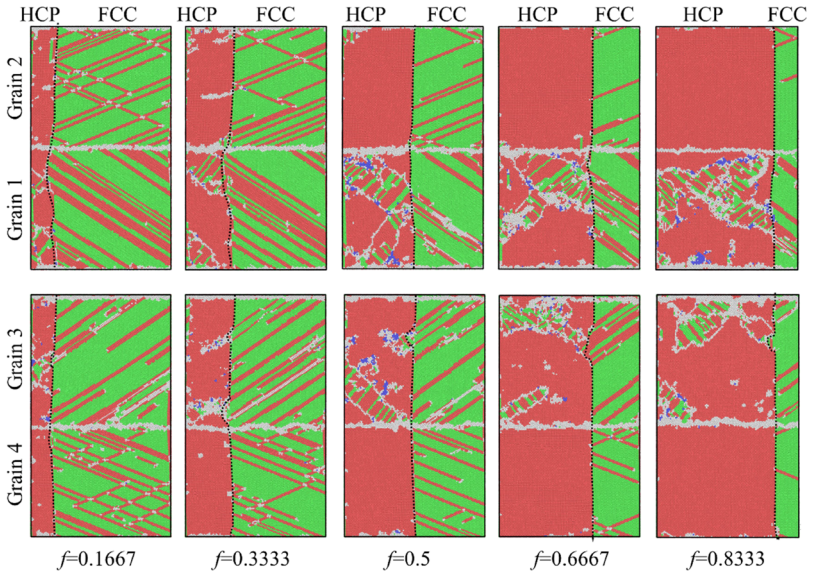

Figure 6. Comparative plastic deformations in the PCNLDP HEAs with various HCP phase volume fractions.

severe plastic deformation in the FCC-phased sample. The solid lines are the variations in the NLDP sample. Neither the increase in FCC-structured atoms nor the decrease in HCP-structured atoms is very significant, indicating that the DP structure has an obvious suppression effect on plastic deformation of the CoCrFeMnNi alloy. In short, the DP strengthening mechanisms include phase strengthening and IPB strengthening, while the softening effects due to IPB migration and dislocation nucleation from the reaction sites should not be ignored.

3.5. Volume Fraction-Dependent Strengthening Mechanism. Since the dimensions of the simulated samples are constant, the increase of HCP phase volume fraction can lead to the increase in thickness of HCP-phased lamella and the decrease in thickness of FCC-phased lamella. While the variations of thickness of the lamellas can significantly affect the plastic deformation of materials, it is essential to comparatively study the plastic deformation in all the NLDP samples for illustrating the phase volume fraction-dependent strengthening mechanisms. Figure 6 gives the snapshots of the micro-defects in the materials at a strain of 10%. With the increase of HCP phase volume fraction, the confinement effect on the movements of dislocations and stacking faults and transition from FCC to HCP phase in the FCC layer is becoming more and more obvious. It is generally accepted that the flow stress of nano-laminated materials will increase with the decrease of lamella thickness when subjected to in-plane loading.[44] It means that increasing the HCP phase volume fraction can result in the increased IPB strengthening effect on the FCC layer. Meanwhile, the interactions between dislocations and IPBs become less frequent due to the less active dislocation behaviors in the thinner FCC layer. As previously mentioned, the migration of IPB originates from the accumulation of dislocations at the IPB. As a result, the migration of IPB becomes more unapparent, indicating that increasing the HCP phase volume fraction can lead to a decreased softening effect due to IPB migration.

To clearly show the phase volume fraction-dependent softening effect induced by IPB migration, we define a IPB-affected zone (phase boundary-affected zone, PBAZ) that contains an atomic layer with 2 nm thickness on both sides of the IPB and count the length of dislocation lines in the PBAZ. Figure 7 shows the length of dislocation lines in the PBAZ as a function of phase volume fraction at a strain of 10%. Obviously, higher volume fraction can lead to fewer IPB dislocations and thus lower displacement of migration of IPB, that is, decreased softening effect due to IPB migration.

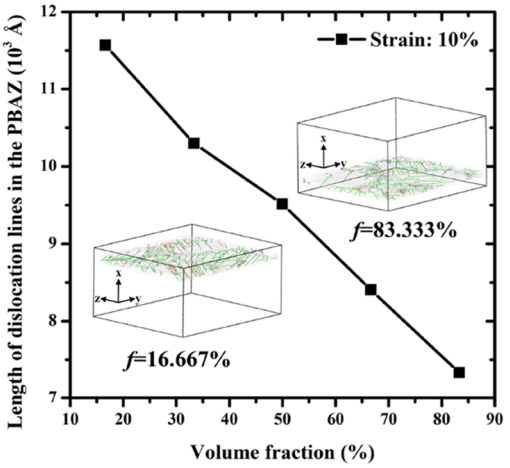

Figure 7. Length of dislocation lines in the phase boundary-affected zone (PBAZ) versus phase volume fraction at a strain of 10%. The insets are two representative snapshots of dislocation microstructures in the PBAZ of the NLDP with phase volume fractions of 16.667 and 83.333%, respectively. The dislocations are detected by DXA.

Increasing HCP phase volume fraction increases the thickness of the HCP layer, which can also affect the plastic behaviors in the HCP layer. It can be seen from Figure 6 that more deformation twins and dislocations emit from the PB and propagate in the HCP layer. As illustrated in Figure 5, the nucleation of deformation twins and dislocations from the sites of dislocation−IPB interaction is a kind of softening factor in the strength of the material. Thus, the higher the phase volume fraction, the higher the softening effect by defect nucleation.

As mentioned above, the boundary of deformation twin, stacking fault, and phase transformation in FCC phase are recognized as one-layered, double-layered, and multilayered

https://doi.org/10.1021/acsomega.2c02027
ACS Omega 2022, 7, 29675−29683

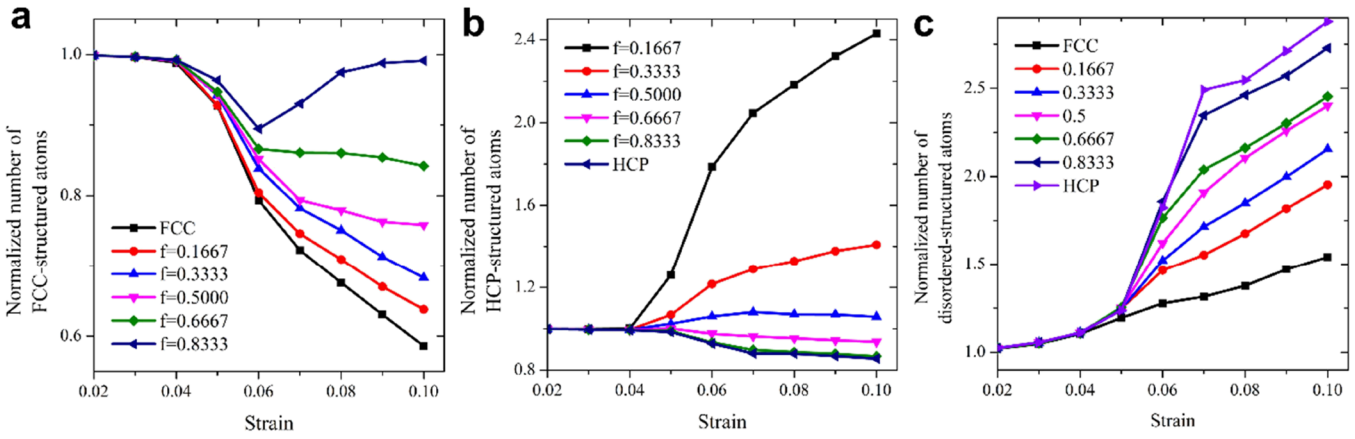

Figure 8. Variations of normalized numbers of FCC-structured, HCP-structured, and disordered atoms with strain.

HCP-structured atoms, those in HCP phase are recognized as one-layered, double-layered, and multilayered FCC-structured atoms, and dislocation cores and amorphizations in both phases are recognized as disordered atoms. Thus, we compute the variations of normalized atomic fractions of FCC-structured, HCP-structured, and disordered atoms with applied strain for further comparative study of plastic deformations in the NLDP with different phase volume fractions, as shown in Figure 8. For the deformation of NLDP with a smaller phase volume fraction, the normalized number of FCC-structured atoms decreases quickly, while the normalized number of HCP-structured atoms increases rapidly, which indicates that the plasticity of FCC layer dominates the plastic deformation of the NLDP with smaller phase volume fraction. On the contrary, for the deformation of NLDP with larger phase volume fraction, the normalized number of FCC-structured atoms decreases slowly (f = 0.6667), and even increases slightly (f = 0.8333), while the normalized number of HCP-structured atoms decreases slightly, which emphasizes the plasticity of the HCP layer in the deformation of the NLDP with a larger phase volume fraction. In addition, the normalized number of disordered atoms increases with the increase of phase volume fraction (Figure 8c), which is the result of increased dislocation−IPB interaction and local amorphization.

The flow stress of the DP HEA can be described by the rule of mixture,[26] that is

$$\sigma = \sigma_{HCP} \cdot f + \sigma_{FCC} \cdot (1 - f) + I_{PB} \tag{3}$$

where σ_{HCP} and σ_{FCC} are the mean flow stress of pure FCC phase and pure HCP phase, respectively, and $I_{FCC-HCP}$ is the interacting stress between the two phases, including PB strengthening and PB softening. Eq 3 can be further written as

$$\sigma = (\sigma_{HCP} - \sigma_{FCC}) \cdot f + \sigma_{FCC} + \sigma_{PB}^{strengthening} - \sigma_{PB}^{softening} \tag{4}$$

The PB strengthening originates from the blocking of PB on dislocation motion in both FCC and HCP lamellas, thus

$$\sigma_{PB}^{strengthening} = k_{FCC} \cdot (\lambda_{FCC} \cdot (1 - f)^{-1} + k_{HCP} \cdot (\lambda_{HCP} \cdot f)^{-1} \tag{5}$$

The PB softening effect is the result of PB migration, which is characterized by the length of dislocation lines in the PBAZ (Figure 7). The length of dislocation lines in the PBAZ and the HCP phase volume fraction have a linear relationship. Thus, the softening effect can be simply written as

$$\sigma_{PB}^{softening} = k \cdot \lambda_{HCP} \cdot (1 - f) = k \cdot L_x \cdot f \cdot (1 - f) \tag{6}$$

Based on the abovementioned analysis, the mechanisms for the volume fraction-dependent flow stress include volume fraction-dependent phase strengthening effect, volume fraction-dependent IPB strengthening effect, and volume fraction-dependent IPB softening effect, that is, IPB migration and dislocation nucleation from the reaction sites. It is known that the flow stress of nano-laminated metallic materials is mainly affected by both the interface and the thickness of the lamella, without considering the effect of phase volume fraction. As the variation of the thickness of the lamella and the density of interfaces, the relationships between the flow stress and the thickness change accordingly.[59−64] In this work, the variation of phase volume fraction would not affect the density of IPBs, but has an opposite effect on the layer thickness of the two phases. Thus, the combined phase strengthening, IPB strengthening, and IPB softening effects contribute jointly to the strength of the NLDP.

4. CONCLUSIONS

In this work, large-scale atomistic simulations of in-plane tension of NLDP HEAs with different HCP phase volume fractions are carried out, aiming to reveal the effect of phase volume fraction on its tensile mechanical properties, as well as the underlying mechanisms. It is found that the DP structure can significantly enhance the strength of the material, and the strength shows apparent phase volume fraction dependence. The yield stress increases monotonously with the increase of phase volume fraction, resulting from the increased inhibition effect of IPB on the nucleation of partial dislocations in the FCC lamella. There exists a critical phase volume fraction, where the flow stress is the largest. The mechanisms for the volume fraction-dependent flow stress include volume fraction-dependent phase strengthening effect, volume fraction-dependent IPB strengthening effect, and volume fraction-dependent IPB softening effect, that is, IPB migration and dislocation nucleation from the dislocation−IPB reaction sites. This work can provide a fundamental understanding for the physical mechanisms of strengthening effects in face-centered cubic HEAs with a nanoscale NLDP structure.

https://doi.org/10.1021/acsomega.2c02027
ACS Omega 2022, 7, 29675−29683

■ ASSOCIATED CONTENT

Supporting Information

The Supporting Information is available free of charge at https://pubs.acs.org/doi/10.1021/acsomega.2c02027.

Generalized stacking fault energies obtained with the MEAM potential and uniaxial tensile stress−strain curves within the elastic deformation obtained with the MEAM potential and first-principles calculations (PDF)

■ AUTHOR INFORMATION

Corresponding Authors

Yin Yao − *Institute of Advanced Structure Technology and Beijing Key Laboratory of Lightweight Multifunctional Composite Materials and Structures, Beijing Institute of Technology, Beijing 100081, China*; Email: yaoyin@bit.edu.cn

Shaohua Chen − *Institute of Advanced Structure Technology and Beijing Key Laboratory of Lightweight Multifunctional Composite Materials and Structures, Beijing Institute of Technology, Beijing 100081, China*; orcid.org/0000-0002-5277-453X; Email: shchen@bit.edu.cn

Author

Cheng Huang − *Institute of Advanced Structure Technology and Beijing Key Laboratory of Lightweight Multifunctional Composite Materials and Structures, Beijing Institute of Technology, Beijing 100081, China*

Complete contact information is available at: https://pubs.acs.org/10.1021/acsomega.2c02027

Author Contributions

Y.Y. and S.C. conceived and supervised the work. C.H. performed the simulations and wrote the paper. All authors discussed the results and revised the manuscript.

Notes

The authors declare no competing financial interest.

■ ACKNOWLEDGMENTS

This work is supported by NSFC (Grant Nos. 12002035, 11872114, and 12032004).

■ REFERENCES

(1) Cheng, Z.; Zhou, H.; Lu, Q.; Gao, H.; Lu, L. Extra strengthening and work hardening in gradient nanotwinned metals. *Science* **2018**, *362*, 1925.

(2) Pan, Q.; Zhou, H.; Lu, Q.; Gao, H.; Lu, L. History-independent cyclic response of nanotwinned metals. *Nature* **2017**, *551*, 214−217.

(3) Li, J.; Lu, W.; Gibson, J.; Zhang, S.; Korte-Kerzel, S.; Raabe, D. Compatible deformation and extra strengthening by heterogeneous nanolayer composites. *Scr. Mater.* **2020**, *179*, 30−35.

(4) Wang, Y.; Li, J.; Lu, W.; Yuan, F.; Wu, X. Enhanced co-deformation of a heterogeneous nanolayered Cu/Ni composite. *J. Appl. Phys.* **2019**, *126*, 215111.

(5) Zhao, S.; Zhang, R.; Chong, Y.; Li, X.; Abu-Odeh, A.; Rothchild, E.; Chrzan, D. C.; Asta, M.; Morris, J. W., Jr.; Minor, A. M. Defect reconfiguration in a Ti-Al alloy via electroplasticity. *Nat. Mater.* **2021**, *20*, 468−472.

(6) Zhao, L.; Guan, B.; Xin, Y.; Huang, X.; Liu, C.; Wu, P.; Liu, Q. A quantitative study on mechanical behavior of Mg alloys with bimodal texture components. *Acta Mater.* **2021**, *214*, No. 117013.

(7) Zhang, Z.; Yang, Z.; Lu, S.; Harte, A.; Morana, R.; Preuss, M. Strain localisation and failure at twin-boundary complexions in nickel-based superalloys. *Nat. Commun.* **2020**, *11*, 4890.

(8) Yeh, J.-W.; Chen, S.-K.; Lin, S.-J.; Gan, J.-Y.; Chin, T.-S.; Shun, T.-T.; Tsau, C.-H.; Chang, S.-Y. Nanostructured high-entropy alloys with multiple principal elements: Novel alloy design concepts and outcomes. *Adv. Eng. Mater.* **2004**, *6*, 299−303.

(9) Cantor, B.; Chang, I. T. H.; Knight, P.; Vincent, A. J. B. Microstructural development in equiatomic multicomponent alloys. *Mater. Sci. Eng., A* **2004**, *375*−*377*, 213−218.

(10) Gludovatz, B.; Hohenwarter, A.; Catoor, D.; Chang, E. H.; George, E. P.; Ritchie, R. O. A fracture-resistant high-entropy alloy for cryogenic applications. *Science* **2014**, *345*, 1153−1158.

(11) Zhang, Y.; Zuo, T. T.; Tang, Z.; Gao, M. C.; Dahmen, K. A.; Liaw, P. K.; Lu, Z. P. Microstructures and properties of high-entropy alloys. *Prog. Mater. Sci.* **2014**, *61*, 1−93.

(12) Li, Z.; Zhao, S.; Ritchie, R. O.; Meyers, M. A. Mechanical properties of high-entropy alloys with emphasis on face-centered cubic alloys. *Prog. Mater. Sci.* **2019**, *102*, 296−345.

(13) Li, J.; Fang, Q.; Liaw, P. K. Microstructures and Properties of High-Entropy Materials: Modeling, Simulation, and Experiments. *Adv. Eng. Mater.* **2020**, *23*, 2170002.

(14) Lu, X.; Zhao, J.; Yu, C.; Li, Z.; Kan, Q.; Kang, G.; Zhang, X. Cyclic plasticity of an interstitial high-entropy alloy: experiments, crystal plasticity modeling, and simulations. *J. Mech. Phys. Solids* **2020**, *142*, No. 103971.

(15) Wei, K.; Yang, Q.; Ling, B.; Yang, X.; Xie, H.; Qu, Z.; Fang, D. Mechanical properties of Invar 36 alloy additively manufactured by selective laser melting. *Mater. Sci. Eng., A* **2020**, *772*, No. 138799.

(16) Zhang, Q.; Huang, R.; Zhang, X.; Cao, T.; Xue, Y.; Li, X. Deformation Mechanisms and Remarkable Strain Hardening in Single-Crystalline High-Entropy-Alloy Micropillars/Nanopillars. *Nano Lett.* **2021**, *21*, 3671−3679.

(17) Yang, T.; Zhao, Y. L.; Tong, Y.; Jiao, Z. B.; Wei, J.; Cai, J. X.; Han, X. D.; Chen, D.; Hu, A.; Kai, J. J.; et al. Multicomponent intermetallic nanoparticles and superb mechanical behaviors of complex alloys. *Science* **2018**, *362*, 933−937.

(18) Zhang, R.; Zhao, S.; Ding, J.; Chong, Y.; Jia, T.; Ophus, C.; Asta, M.; Ritchie, R. O.; Minor, A. M. Short-range order and its impact on the CrCoNi medium-entropy alloy. *Nature* **2020**, *581*, 283−287.

(19) Shi, P.; Li, R.; Li, Y.; Wen, Y.; Zhong, Y.; Ren, W.; Shen, Z.; Zheng, T.; Peng, J.; Liang, X.; et al. Hierarchical crack buffering triples ductility in eutectic herringbone high-entropy alloys. *Science* **2021**, *373*, 912−918.

(20) Wei, S.; Kim, S. J.; Kang, J.; Zhang, Y.; Zhang, Y.; Furuhara, T.; Park, E. S.; Tasan, C. C. Natural-mixing guided design of refractory high-entropy alloys with as-cast tensile ductility. *Nat. Mater.* **2020**, *19*, 1175−1181.

(21) Li, W.; Xie, D.; Li, D.; Zhang, Y.; Gao, Y.; Liaw, P. K. Mechanical behavior of high-entropy alloys. *Prog. Mater. Sci.* **2021**, *118*, No. 100777.

(22) Zhang, Q.; Huang, R.; Jiang, J.; Cao, T.; Zeng, Y.; Li, J.; Xue, Y.; Li, X. Size effects and plastic deformation mechanisms in single-crystalline CoCrFeNi micro/nanopillars. *J. Mech. Phys. Solids* **2022**, *162*, 162.

(23) Lei, Z.; Liu, X.; Wu, Y.; Wang, H.; Jiang, S.; Wang, S.; Hui, X.; Wu, Y.; Gault, B.; Kontis, P.; et al. Enhanced strength and ductility in a high-entropy alloy via ordered oxygen complexes. *Nature* **2018**, *563*, 546−550.

(24) Ding, Q.; Zhang, Y.; Chen, X.; Fu, X.; Chen, D.; Chen, S.; Gu, L.; Wei, F.; Bei, H.; Gao, Y.; et al. Tuning element distribution, structure and properties by composition in high-entropy alloys. *Nature* **2019**, *574*, 223−227.

(25) Yang, Y.; Chen, T.; Tan, L.; Poplawsky, J. D.; An, K.; Wang, Y.; Samolyuk, G. D.; Littrell, K.; Lupini, A. R.; Borisevich, A.; et al. Bifunctional nanoprecipitates strengthen and ductilize a medium-entropy alloy. *Nature* **2021**, *595*, 245−249.

(26) Fang, Q.; Chen, Y.; Li, J.; Jiang, C.; Liu, B.; Liu, Y.; Liaw, P. K. Probing the phase transformation and dislocation evolution in dual-phase high-entropy alloys. *Int. J. Plast.* **2019**, *114*, 161−173.

(27) Chen, Y.; Chen, D.; An, X.; Zhang, Y.; Zhou, Z.; Lu, S.; Munroe, P.; Zhang, S.; Liao, X.; Zhu, T.; et al. Unraveling dual phase transformations in a CrCoNi medium-entropy alloy. *Acta Mater.* **2021**, *215*, No. 117112.
(28) Huang, C.; Yao, Y.; Peng, X.; Chen, S. Plastic deformation and strengthening mechanism of FCC/HCP nano-laminated dual-phase CoCrFeMnNi high entropy alloy. *Nanotechnology* **2021**, *32*, 5724.
(29) Li, Z.; Pradeep, K. G.; Deng, Y.; Raabe, D.; Tasan, C. C. Metastable high-entropy dual-phase alloys overcome the strength-ductility trade-off. *Nature* **2016**, *534*, 227−230.
(30) Li, Z.; Körmann, F.; Grabowski, B.; Neugebauer, J.; Raabe, D. Ab initio assisted design of quinary dual-phase high-entropy alloys with transformation-induced plasticity. *Acta Mater.* **2017**, *136*, 262−270.
(31) Zhang, T.; Zhao, R. D.; Wu, F. F.; Lin, S. B.; Jiang, S. S.; Huang, Y. J.; Chen, S. H.; Eckert, J. Transformation-enhanced strength and ductility in a FeCoCrNiMn dual phase high-entropy alloy. *Mater. Sci. Eng., A* **2020**, *780*, No. 139182.
(32) Tracy, C. L.; Park, S.; Rittman, D. R.; Zinkle, S. J.; Bei, H.; Lang, M.; Ewing, R. C.; Mao, W. L. High pressure synthesis of a hexagonal close-packed phase of the high-entropy alloy CrMnFeCo-Ni. *Nat. Commun.* **2017**, *8*, 15634.
(33) Lu, W.; Liebscher, C. H.; Dehm, G.; Raabe, D.; Li, Z. Bidirectional Transformation Enables Hierarchical Nanolaminate Dual-Phase High-Entropy Alloys. *Adv. Mater.* **2018**, *30*, No. e1804727.
(34) Chen, S.; Oh, H. S.; Gludovatz, B.; Kim, S. J.; Park, E. S.; Zhang, Z.; Ritchie, R. O.; Yu, Q. Real-time observations of TRIP-induced ultrahigh strain hardening in a dual-phase CrMnFeCoNi high-entropy alloy. *Nat. Commun.* **2020**, *11*, 826.
(35) Chen, Y.; An, X.; Zhou, Z.; Munroe, P.; Zhang, S.; Liao, X.; Xie, Z. Size-dependent deformation behavior of dual-phase, nanostructured CrCoNi medium-entropy alloy. *Sci. China Mater.* **2020**, *64*, 209−222.
(36) Zhao, S.; Li, Z.; Zhu, C.; Yang, W.; Zhang, Z.; Armstrong, D.; Grant, P.; Ritchie, R.; Meyers, M. Amorphization in extreme deformation of theCrMnFeCoNi high-entropy alloy. *Sci. Adv.* **2021**, *7*, 3108−3137.
(37) Li, X.; Yin, S.; Oh, S. H.; Gao, H. Hardening and toughening mechanisms in nanotwinned ceramics. *Scr. Mater.* **2017**, *133*, 105−112.
(38) Huang, C.; Peng, X.; Yang, B. Effect of heterointerface on the indentation behavior of nano-laminated c-BN/diamond composites. *Ceram. Int.* **2021**, *47*, 28659−28668.
(39) Huang, C.; Yang, B.; Peng, X.; Chen, S. Plastic Deformation and Hardening Mechanisms of a Nano-twinned Cubic Boron Nitride Ceramic. *ACS Appl. Mater. Interfaces* **2020**, *12*, 50161−50175.
(40) Yang, B.; Tong, K.; Huang, C.; Qi, Z.; Yin, D.; Wei, Q.; Zhao, Z.; Peng, X.; Hu, N. Strengthening effects of penetrating twin boundary and phase boundary in polycrystalline diamond. *Diamond Relat. Mater.* **2021**, *117*, No. 108436.
(41) Yang, Y.; Song, Z.; Lu, G.; Zhang, Q.; Zhang, B.; Ni, B.; Wang, C.; Li, X.; Gu, L.; Xie, X.; et al. Intrinsic toughening and stable crack propagation in hexagonal boron nitride. *Nature* **2021**, *594*, 57−61.
(42) Cao, F.-H.; Wang, Y.-J.; Dai, L.-H. Novel atomic-scale mechanism of incipient plasticity in a chemically complex CrCoNi medium-entropy alloy associated with inhomogeneity in local chemical environment. *Acta Mater.* **2020**, *194*, 283−294.
(43) Nishiyama, Z. *Martensitic Transformation*; Academic Press: New York, 1978.
(44) Zhou, H.; Li, X.; Qu, S.; Yang, W.; Gao, H. A jogged dislocation governed strengthening mechanism in nanotwinned metals. *Nano Lett.* **2014**, *14*, 5075−5080.
(45) Plimpton, S. Fast parallel algorithms for short-range molecular dynamics. *J. Comput. Phys.* **1995**, *117*, 1−19.
(46) Choi, W.-M.; Jo, Y. H.; Sohn, S. S.; Lee, S.; Lee, B.-J. Understanding the physical metallurgy of the CoCrFeMnNi high-entropy alloy: an atomistic simulation study. *npj Comput. Mater.* **2018**, *4*, 1.
(47) Li, J.; Xie, B.; Fang, Q.; Liu, B.; Liu, Y.; Liaw, P. K. High-throughput simulation combined machine learning search for optimum elemental composition in medium entropy alloy. *J. Mater. Sci. Technol.* **2021**, *68*, 70−75.
(48) Qi, Y.; Zhao, M.; Feng, M. Molecular simulation of microstructure evolution and plastic deformation of nanocrystalline CoCrFeMnNi high-entropy alloy under tension and compression. *J. Alloys Compd.* **2021**, *851*, No. 156923.
(49) Qi, Y.; Chen, X.; Feng, M. Molecular dynamics-based analysis of the effect of voids and HCP-Phase inclusion on deformation of single-crystal CoCrFeMnNi high-entropy alloy. *Mater. Sci. Eng., A* **2020**, *791*, No. 139444.
(50) Qiu, Y.; Qi, Y.; Zheng, H.; He, T.; Feng, M. Atomistic simulation of nanoindentation response of dual-phase nanocrystalline CoCrFeMnNi high-entropy alloy. *J. Appl. Phys.* **2021**, *130*, 125102.
(51) Stukowski, A. Visualization and analysis of atomistic simulation data with OVITO−the Open Visualization Tool. *Modell. Simul. Mater. Sci. Eng.* **2010**, *18*, No. 015012.
(52) Stukowski, A.; Bulatov, V. V.; Arsenlis, A. Automated identification and indexing of dislocations in crystal interfaces. *Modell. Simul. Mater. Sci. Eng.* **2012**, *20*, No. 085007.
(53) Larsen, P. M.; Schmidt, S.; Schiøtz, J. Robust structural identification via polyhedral template matching. *Modell. Simul. Mater. Sci. Eng.* **2016**, *24*, No. 055007.
(54) Wei, Y. Scaling of maximum strength with grain size in nanotwinned fcc metals. *Phys. Rev. B* **2011**, *83*, No. 132104.
(55) Asaro, R. J.; Krysl, P.; Kad, B. Deformation mechanism transitions in nanoscale fcc metals. *Philos. Mag. Lett.* **2003**, *83*, 733−743.
(56) Asaro, R. J.; Suresh, S. Mechanistic models for the activation volume and rate sensitivity in metals with nanocrystalline grains and nano-scale twins. *Acta Mater.* **2005**, *53*, 3369−3382.
(57) Zhu, T.; Gao, H. Plastic deformation mechanism in nanotwinned metals: An insight from molecular dynamics and mechanistic modeling. *Scr. Mater.* **2012**, *66*, 843−848.
(58) Ming, K.; Li, B.; Bai, L.; Jiang, P.; Wu, X.; Zheng, S.; Wang, J. Dynamically reversible shear transformations in a CrMnFeCoNi high-entropy alloy at cryogenic temperature. *Acta Mater.* **2022**, *232*, No. 117937.
(59) Wang, J.; Misra, A. An overview of interface-dominated deformation mechanisms in metallic multilayers. *Curr. Opin. Solid State Mater. Sci.* **2011**, *15*, 20−28.
(60) Ovid'ko, I. A.; Valiev, R. Z.; Zhu, Y. T. Review on superior strength and enhanced ductility of metallic nanomaterials. *Prog. Mater. Sci.* **2018**, *94*, 462−540.
(61) Zhu, Y.; Li, Z.; Huang, M.; Liu, Y. Strengthening mechanisms of the nanolayered polycrystalline metallic multilayers assisted by twins. *Int. J. Plast.* **2015**, *72*, 168−184.
(62) Doan, D.-Q.; Fang, T.-H.; Chen, T.-H. Interfacial and mechanical characteristics of TiN/Al composites under nano-indentation. *Int. J. Solids Struct.* **2021**, 226−227.
(63) Bu, Y.; Wang, H. Short-range order in multicomponent alloys. *Adv. Mech.* **2021**, *51*, 915−919.
(64) Li, X.; Yan, Z.; Liu, Z.; Zhuang, Z. Advanced structural material design based on simulation and data-driven method. *Adv. Mech.* **2021**, *51*, 82−105.

https://doi.org/10.1021/acsomega.2c02027
ACS Omega 2022, 7, 29675−29683